Proceedings of the 9th U.S. National and 10th Canadian Conference on Earthquake Engineering
Compte Rendu de la 9ième Conférence Nationale Américaine et
10ième Conférence Canadienne de Génie Parasismique
July 25-29, 2010, Toronto, Ontario, Canada • Paper No 1172

DYNAMIC COLLAPSE OF REINFORCED CONCRETE COLUMNS

C. L. Wu[1], Y. S. Yang[2], S.J. Hwang[3] and C. H. Loh[3]

ABSTRACT

This paper presents shaking table test observations of a complete spectrum of major column failure modes, i.e., shear, flexure-shear and flexure failures under moderate axial load. A comparison of test results and existing assessment models, including ASEC/SEI 41-06 Update and Zhu et al. probabilistic model, shows that satisfactory strength predictions and successful identification of column failure modes have been achieved in ASCE/SEI 41-06 Update, which also provides reasonable estimates of load-deformation relations and is useful for identifying older concrete buildings that are at high risk of structural collapse in severe seismic events. The 16th-percentile backbone curve produced by Zhu et al. probabilistic model roughly coincides with the ASCE/SEI 41-06 Update prediction; thus, the ASCE/SEI 41-06 updated provisions appropriately yield a good match with test data while preserving a moderate degree of conservatism.

Introduction

The loss of gravity load carrying capacity of reinforced concrete columns is the most critical factor leading to catastrophic structural collapse of buildings, and thereby causes tragic consequence of losses of lives; for instance, a large number of pancake type of building failures found in the 1999 Chi-Chi (Taiwan) and the 2008 Wenchuan (China) earthquakes, etc., which can be attributed to nonductile detailing fairly common in older concrete columns. To better understand full range structural behavior of a wide variety of concrete columns, a good number of collapse tests using a shaking table have been conducted during the past few years at the National Center for Research on Earthquake Engineering of Taiwan since 2004 to experimentally observe three major types of column failure mechanisms, i.e., flexure, flexure-shear and pure shear failures in a dynamic manner (Fig. 1). The dynamic test data can serve as a great testbed for validating numerical nonlinear simulation methods as well as existing simplified assessment models. The test specimens were a single-story shear frame containing multiple columns (two, three, or four) interconnected at column top through a rigid beam to either allow or prohibit an alternative path for vertical load redistribution using different combinations of ductile and nonductile columns. The ones prohibiting vertical load redistribution using test frames having two identical concrete

[1] Associate Research Fellow, National Center for Research on Earthquake Engineering, Taipei City, 10668, Taiwan
[2] Assistant Professor, Dept. of Civil Engineering, National Taipei University of Technology, Taipei City, Taiwan
[3] Professor, Dept. of Civil Engineering, National Taiwan University, Taipei City, 10668, Taiwan

columns can be considered very similar to quasi-static reversed cyclic tests on double-curvature single columns.

Existing older buildings in high risk of structural collapse during severe seismic events should be retrofitted, but the retrofitting cost of older buildings to comply with current seismic codes could be fairly expensive. Nonetheless, the retrofitting cost may be reduced to an affordable level if a reliable analysis tool with consideration of structural post-peak behavior can be developed to yield accurate prediction of structural failure under extreme seismic events. Collapse simulation in experimental and/or numerical manner can yield important information on the worst scenario that might be encountered in buildings during a very rare earthquake event, and collapse test data is very helpful in facilitating the development of reliable analysis tools. Moreover, probability of structural collapse in older concrete buildings during severe earthquake events might be relatively low (less than 10%) according to the statistics reported by Otani (1999). A plausible conclusion is that if resources can be focused on buildings that are most vulnerable to collapse, and inexpensive retrofitting methods are provided accordingly, then seismic risk and fatalities can be significantly reduced at affordable costs. A key task is then to effectively identify buildings that are vulnerable to earthquake damage or collapse. This paper reports research findings from the shear frames containing two concrete columns of an identical design, in which gravity load redistribution was not allowed for both columns failed at the same time. Listed in Table 1 are the main characteristics of selected column specimens tested in the past on shaking table at NCREE. Their full-range structural behavior will be discussed in the following sections.
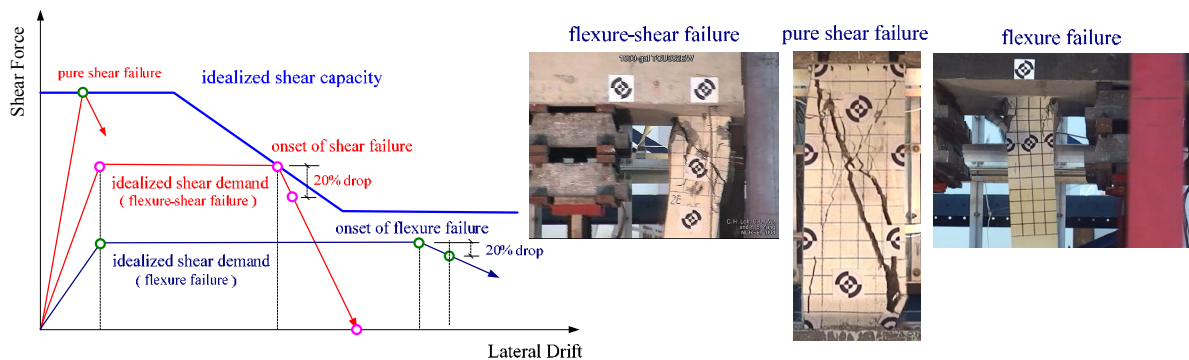

Figure 1.   Conceptual illustration of major column failure modes and selected damage photos taken from shaking table tests at NCREE.

Table 1.   Main characteristics of column specimens

Column Type	Dimension (cm*cm)	Clear Height (cm)	ρ_1	ρ_v	$P/f_c'A_g$	Transverse Ties	Input Motion
FS	20*20	173	1.4%	0.1%	10.1%	90° end hook	TCU076ns
FS	20*20	173	1.4%	0.1%	10.4%	90° end hook	TCU082ew
F	20*20	173	1.4%	0.25%	10.4%	135° end hook	TCU076ns
F	20*20	173	1.4%	0.25%	10.4%	135° end hook	TCU082ew
S	25*25	75	3.2%	0.07%	9.7%	90° end hook	TCU082ew
S	25*25	100	3.2%	0.07%	6.8%	90° end hook	TCU082ew

Note: "FS" = Flexure-Shear critical column; "F" = Flexure critical column; "S" = Shear critical column

Testing Program

The experimental setup of specimen frames on the shaking table is shown in Fig. 2. To cut down the experimental cost for testing various types of double-curvature concrete columns on a shaking table, the de-attachable rigid steel loading beam (Fig. 2b) has been used in recent years to replace the original concrete mega beam setup introduced in 2004 (Fig. 2a) as the steel loading beam can be reused with no extra cost. Either way, the experimental setup aims for instrumented observation of global dynamic collapse of the columns. The concrete frame was braced by frictionless sliders of the steel supporting frame at the rigid beam level to be restrained from out-of-plane movement while the frictionless sliders allowed the concrete frame to move freely in both lateral and vertical directions. The steel supporting frame contained diagonal bracings in the out-of-plane direction. A pair of parallel steel protective beams (Fig. 2a) ran underneath the mega concrete beam to catch the concrete frame when collapse occurred such that abrupt impact to the shaking table could be avoided. Another type of protective device was to use the steel catching chain above the mega loading beam (Fig. 2b). The heavy mega beam and lead packets comprised the gravity load to concrete columns, the initial axial load ratio of which varied from 6.8% to 10.4% $f_c'A_g$ considered as in the moderate gravity load level to cause incipient tension failure of longitudinal reinforcement. The column specimens tested in the past few years had aspect ratios varying from 3 to 8.7 to cover a complete spectrum of major column failure modes shown in Fig. 1.
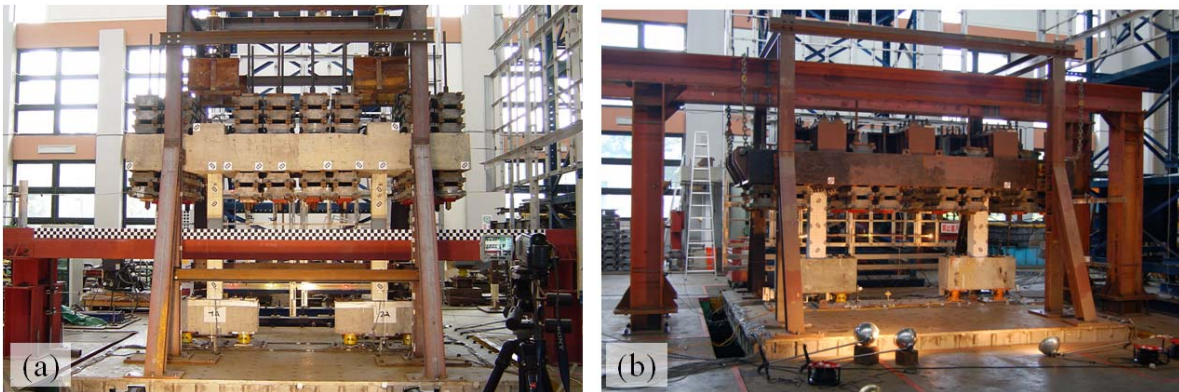

Figure 2.   Photographical view of the experimental setup: (a) typical concrete frame; (b) de-attachable steel loading beam on the top of concrete columns.
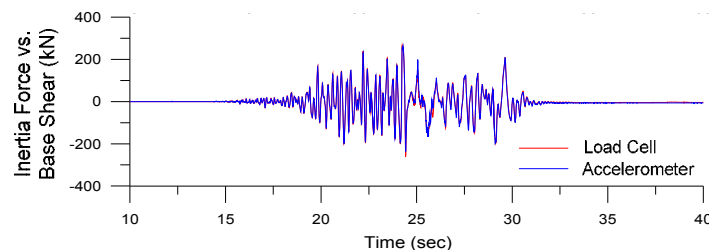

Figure 3.   Comparison of base shear time histories of test frame obtained from accelerometers and load cells.

Specimen instrumentation consisted of load cells, accelerometers, Temposonics II and string pot linear displacement transducers (LDTs), strain gauges, and digital image-based

displacement measurement system to collect valuable experimental data of engineering interest. Strain gauges were applied to the surface of longitudinal and transverse reinforcing bars in columns, beams, and joints when construction was still in progress to reveal information on locations and time instants of bar yielding during tests. Accelerometers measured lateral, transverse and vertical accelerations at specified locations of interest, in particular, at the top of columns. Load cells measured column axial load, in-plane and out-of-plane shear forces. Column shear force is the lateral force measured by two load cells installed underneath the footing minus the inertia force induced at the footing. Column axial load is the vertical force measured by two load cells minus the footing weight. Base shear is the sum of column shear forces, representing the frame shear at the footing level. Bending moment at the column base was determined using free-body equilibrium of the footing, including the shear and axial force outputs from load cells. Displacement transducers and digital image-based measurement system were employed to measure global frame deformations in both vertical and horizontal directions. The base-shear response of the frame can be obtained either from accelerometers installed on the mass at the top of the frame or from load cells installed underneath the footings of columns. These data were compared to ensure the functionality of frictionless sliders installed on the steel out-of-plane supporting frame. These two curves basically had good agreement up to the point of column failure; one of such plots is shown in Fig. 3.

Table 2. Main characteristics of selected ground motion records in the 1999 Chi-Chi earthquake employed to excite test frames.

Station	Direction	Site Class	Lat. (°N)	Long. (°E)	Elev. (m)	R_{ep} [1] (km)	R_{jb} [2] (km)	R_{rup} [3] (km)	PGA (cm/s^2)	PGV (cm/s)	PGD (cm)
TCU076	NS	D	23.908	120.676	100	13.7	2.99	3.17	420	-63.02	-72.79
TCU082	EW	D	24.148	120.676	80	34.2	4.35	4.47	221	-51.54	152.60

[1] R_{ep} = the distance from the station to the earthquake epicenter
[2] R_{jb} = the Joyner-Boore shortest distance from the station to the vertical projection of the rupture surface
[3] R_{rup} = the shortest distance from the station to the rupture surface

Prior to the earthquake simulation tests, the test frames were subjected to low level (20-30cm/sec^2) white noise excitation lasting for 90sec so that the natural periods and viscous damping ratios of the virgin frames could be numerically identified using a transfer function between the top and base of the test frame. The determined natural periods of test frames varied from 0.1sec to 0.47sec. Because a reduced scale factor of one-half was assigned to the test frame due to facility constraints, the input ground motion was then adjusted using a time compression factor (i.e., square root of the reduced scale factor) on the basis of keeping unchanged the acceleration scale factor (i.e., equal to one). The disadvantage was that the time compression factor induced a higher strain rate than real earthquakes. In the past tests, the NS component of TCU076 accelerogram and the EW component of TCU082 accelerogram from the 1999 Chi-Chi Taiwan earthquake were used as input ground motions based on the following considerations:

- The two stations are located in central Taiwan, and are in the right proximity of the typical prototype buildings studied herein.
- These two records are representative of main characteristics of ordinary (TCU082) and near-fault (TCU076) earthquake motions in central Taiwan. TCU076 and TCU082 were near-fault stations in the 1999 Chi-Chi earthquake as indicated in Table 2, but the strong ground shaking recorded at station TCU082 did not contain velocity pulses or static fling step pulse, which might be observed in a near-fault site. In contrast, TCU076 motion

contains dynamic velocity pulses. The occurrence frequency of velocity pulses in a near-fault zone remains a mystery due to the very limited near-fault motion data collected and research findings up to date. The static fling effect is beyond the scope of this study. Distinct from the narrow band nature of intermediate-period velocity pulses existing in TCU076 (Fig.4a), TCU082 has broader frequency contents (Fig. 4b) and excitation force was able to remain approximately at the same intensity level even when columns sustained initial damage and minor cracking, and the structural period already started to lengthen.
- Spectral values of selected ground motions had to meet the capacity limitation of the shaking table testing system.
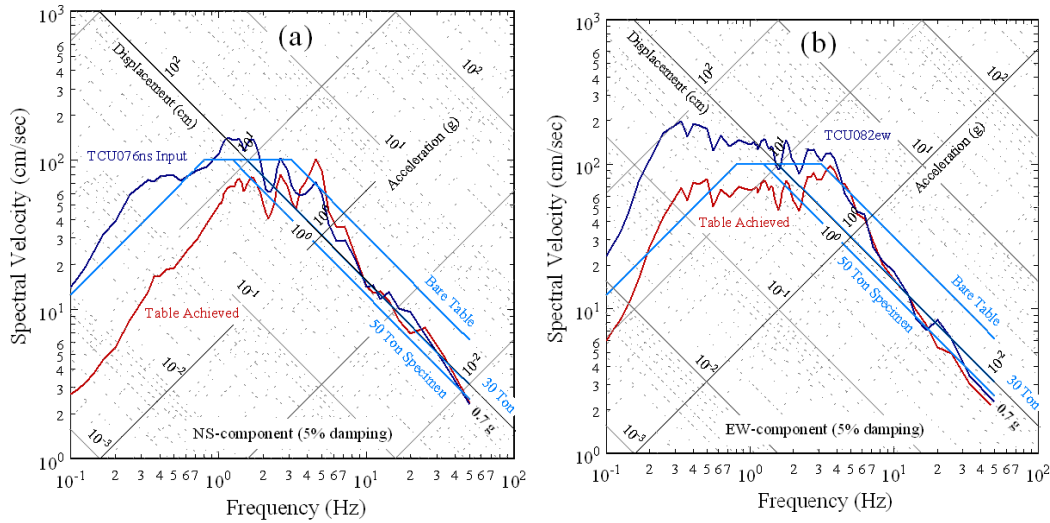

Figure 4. Tripartite response spectra of table achieved motions applied to flexure-shear critical columns at 0.63g in solid red lines: (a) TCU076ns; (b) TCU082ew. Also shown are table performance curves (light blue) and target response spectra (blue).

The selected ground motions, after being modified with a trapezoidal frequency domain filter from 0.2Hz to 20Hz, were scaled to different PGA levels ranging from 0.4g to 2.0g until global collapse had been observed. Sample response spectra of the achieved table motions are presented in Fig. 4. Both stations have a local site condition of Type D, which is usually categorized as stiff soil with shear wave velocity of approximately 180-360m/sec. The table performance curve, including maximum displacement, maximum velocity, and maximum acceleration for a given operating frequency either with a bare table or with a specimen payload, is also provided in the figure. It is seen that even though there were discrepancies between the target and achieved table motions in the range of lower frequencies due to technical reasons, the achieved motions basically demonstrated the motion signature that the authors would like to deliver; i.e., the narrow band pulse in achieved TCU076 motion (Fig. 4a) and broadband waveforms in achieved TCU082 motion (Fig. 4b).

Introduction of Existing Assessment Models

ASCE/SEI 41-06 is the most recent seismic rehabilitation standard published in 2007. Its Table 6-8 provides modeling parameters and numerical acceptance criteria for nonlinear analysis of RC columns. Subsequent to development of the provisions, various studies have found that

the provisions produce satisfactory estimates for lateral strength, but in many cases they considerably underestimate drifts at effective yield, shear failure, and axial failure. Using results of these studies and explicit consideration of response statistics, Elwood et al. (2007) proposed revisions for Table 6-8 in ASCE/SEI 41-06 (referred to as "ASCE/SEI 41-06 Update" hereafter) so that accuracy in seismic assessments can be substantially improved, while maintaining an appropriate confidence of achieving the desired performance objective. ASCE/SEI 41-06 calculates plastic flexural moment strength of RC columns using expected material properties. Nominal shear strength is calculated using the following equation:

$$V_{41} = k\frac{A_{st}f_y d}{s} + \lambda k\left(\frac{0.5\sqrt{f_c'}}{M/Vd}\sqrt{1+\frac{P}{0.5\sqrt{f_c'}A_g}}\right)0.8A_g \quad (\text{MPa})$$

(1)

in which $k = 1$ in regions of low ductility demand (i.e., $\mu_\Delta \leq 2$), $k = 0.7$ in regions of high ductility demand (i.e., $\mu_\Delta \geq 6$), and k varies linearly between these limits; $\lambda = 1$ for normal weight aggregate concrete and 0.75 for lightweight aggregate concrete; P is axial compression force (= 0 for tension force); A_g denotes gross cross-sectional area of column; f_c' is the concrete compressive strength; d is effective depth (defined as the depth to the centroid of the tensile reinforcement, permitted to assume $d = 0.8h$, where h is the dimension of the column in the direction of shear); M and V are moment and shear at section of maximum moment under design loadings, and the value of M/Vd shall not be taken greater than 4 or less than 2.

While mechanics-based models may be preferable for predicting the hysteretic response of nonductile columns, such models have not been shown to provide an adequate representation of columns with very light transverse reinforcement and susceptible to shear failure. Elwood and Moehle (2006) proposed empirical formulae to predict drift capacities of columns at different limit states (flexural yielding, shear failure, axial failure) so that an idealized backbone curve as shown in Fig. 1 can be readily constructed. Their predictive equations are suitable for columns experiencing a flexure-shear failure mode. These empirical equations were later modified by Zhu et al. (2007) with an expanded database and the inclusion of uncertainty in drift capacity estimates for flexure-shear columns at shear and axial failure, as well as flexural columns at flexural failure. Column classification methods were also developed accordingly to enable end users to determine which type of failure is more likely to occur so that the respective set of empirical equations can be employed to generate a predictive backbone curve. In the idealized backbone curve of Fig. 1, the peak shear strength of a column is determined from its plastic moment strength based on standard section analysis. It is noted that the equation for predicting drift at flexural yield includes flexibility due to bar slip from the footing or beam-column joint, and can be found in Elwood and Moehle (2006). Based on Zhu et al. (2007), the median prediction of lateral drift at shear failure takes the form:

$$\left(\delta_s\right)_{median} = 2.02\rho'' - 0.025\frac{s}{d} + 0.013\frac{a}{d} - 0.031\frac{P}{A_g f_c'}$$

(2)

$\rho'' = A_{st}/bs$ is the transverse reinforcement ratio; A_{st} is the cross-sectional area of transverse reinforcement parallel to the applied shear along one principal direction of the cross section; b is

the width of column section; s is the hoop spacing; a is shear span. The median prediction of lateral drift at axial failure takes the form (Zhu et al., 2007):

$$\left(\delta_a\right)_{median} = 0.184 \exp\left(-1.45\mu\right) \tag{3}$$

in which the effective coefficient of friction μ is given by:

$$\mu = \frac{P/F_{st} - 1}{\left(P/2.1F_{st}\right) + 2.1} \tag{4}$$

where $F_{st} = A_{st} f_{yt} d_c / s$ is the shear resistance provided by the transverse reinforcement using a 45º truss model; f_{yt} is the yield stress of the transverse reinforcement; d_c is the depth of column core from centerline to centerline of the transverse ties; the constant of 2.1 comes from an underlying assumption of columns with low transverse reinforcement. For flexure-dominated columns, the median prediction of lateral drift at flexure failure is determined by (Zhu et al., 2007):

$$\left(\delta_f\right)_{median} = 0.049 + 0.716\rho_l + 0.120\frac{\rho'' f_{yt}}{f_c'} - 0.042\frac{s}{d} - 0.070\frac{P}{A_g f_c'} \tag{5}$$

$\rho_l = A_{sl}/bh$ is the longitudinal reinforcement ratio; A_{sl} is the total area of longitudinal reinforcement. In passing, it is mentioned that Zhu et al. (2007) did not propose empirical predictive formulae for constructing the backbone curve of pure shear failure.

Test Observations and Comparison with Assessment Models

Hysteretic data collected from the shaking table tests are compared with the aforementioned predictive models. In addition to providing more reversed cyclic data, which is essential for validating existing analytical models, dynamic test results can also contribute to evaluating the ability of the models to predict dynamic structural response due to seismic excitations. The ability of nonlinear dynamic analysis models to capture the observed structural response was explored in the authors' other papers, e.g., Yang et al. (2006), Yavari et al. (2009), etc. Major differences between dynamic and static tests include the strain rate effect and varied loading history determined by dynamic response of the specimen to the input base motion. The experimental hysteretic loops shown in Figs. 5-7 represent frame base shear vs. frame lateral drift responses of flexure-shear, flexure, and shear critical columns, respectively, which are a direct summation of individual column hysteretic curves to remove the shear asymmetry due to overturning moment induced axial forces.

The ASCE/SEI 41-06 Update proposed the failure mode classification scheme for RC columns using a variable matrix containing nominal shear strength V_{41}, plastic shear demand V_{Mp} and the transverse reinforcement detailing (Table 3). Its classification scheme successfully identifies all the observed failure modes of columns reported in this paper. The column drift at flexural yield obtained from the Update assumes an effective flexural rigidity of $0.3E_cI_g$, which corresponds to only 60% of the value originally assumed in ASCE/SEI 41-06 (2007). The reduced stiffness incorporates the influence of bar slip prior to yielding of the longitudinal

reinforcement and thereby provides a better agreement with the recorded data. The effective shear rigidity is assumed to be $0.4E_cA_g$. The second model to be included for comparison is the probabilistic backbone curve proposed by Zhu *et al.* (2007). The column classification method of that model also successfully identifies the observed failure modes of all columns reported in this paper. The lateral drift ratio at flexural yield was considered as the sum of lateral displacements due to flexure, shear, and bar slip of the column divided by the clear column height. Median values were used to compute drifts at shear and axial failure of flexure-shear critical columns, and drifts at flexural failure of flexural columns. It should be mentioned that Zhu et al. (2007) does not propose assessment models for shear critical columns, so only the predictive curves from the ASCE/SEI 41-06 Update are reported in Fig. 7. The assessment models were derived from test data on isolated columns under reversed cyclic loadings of a lower strain rate than real earthquakes without loading pattern variation, which likely accounts for some of the discrepancy between calculated and measured values. Overall, the ASCE/SEI 41-06 Update appropriately yields a satisfactory match with column test data of flexure-shear and flexure failures while preserving a moderate degree of conservatism.

Table 3.   Classification of columns for determination of modeling parameters (modified from Elwood et al., 2007)

	Transverse Reinforcement Details		
	ACI conforming details with 135° hooks	Closed hoops with 90° hooks	Other (including lap spliced transverse reinforcement)
$V_{M_p}/(V_{41}/k) \leq 0.6$	Flexural failure	Flexural-shear failure	Flexural-shear failure
$1.0 \geq V_{M_p}/(V_{41}/k) > 0.6$	Flexural-shear failure	Flexural-shear failure	Shear failure
$V_{M_p}/(V_{41}/k) > 1.0$	Shear failure	Shear failure	Shear failure

Note: k represents a modifier based on ductility demand, defined in ASCE/SEI 41-06.

Fig. 5 compares the predictive flexure-shear backbone curves obtained from the ASCE/SEI 41-06 Update and Zhu et al. (2007) models with test data. The 16th-percentile curve of Zhu *et al.* (2007) coincides roughly with estimates from the ASCE/SEI 41-06 Update. The median flexural strength curves are presented in Fig. 6 as solid red lines. After the onset of flexural failure of flexural columns (shown as red hollow circles in Fig. 6), P-Δ effects will dominate the response; thereby strength degradation after that point was estimated using the measured initial axial load multiplied by the measured drift ratio as the slope of the post-peak descending branch (shown as inclined solid red lines in Fig. 6) with its probability band (16th- and 84th-percentile values shown as dashed red lines) reported as well. Fig. 6 reveals that dynamic hysteretic response under TCU076 near-fault motion is very similar to a push over curve due to low-cycle failure, while dynamic hysteretic response under TCU082 motion is not captured by the nonlinear static procedure due to the observed cyclic degradation of lateral strength, in which case time history analysis shall be desirable. Fig. 7 suggests that the ASCE/SEI 41-06 Update yields satisfactory shear strength estimates, but overestimates the effective shear stiffness. The experimental post-peak branch has a slower descending slope than estimate from the ASCE/SEI 41-06 Update because a higher longitudinal steel ratio of 3.2% was used. In case of 1.4% longitudinal steel ratio, pure shear failure caused a steeper drop of strength and no residual strength was observed according to other cyclic test data collected by the authors.
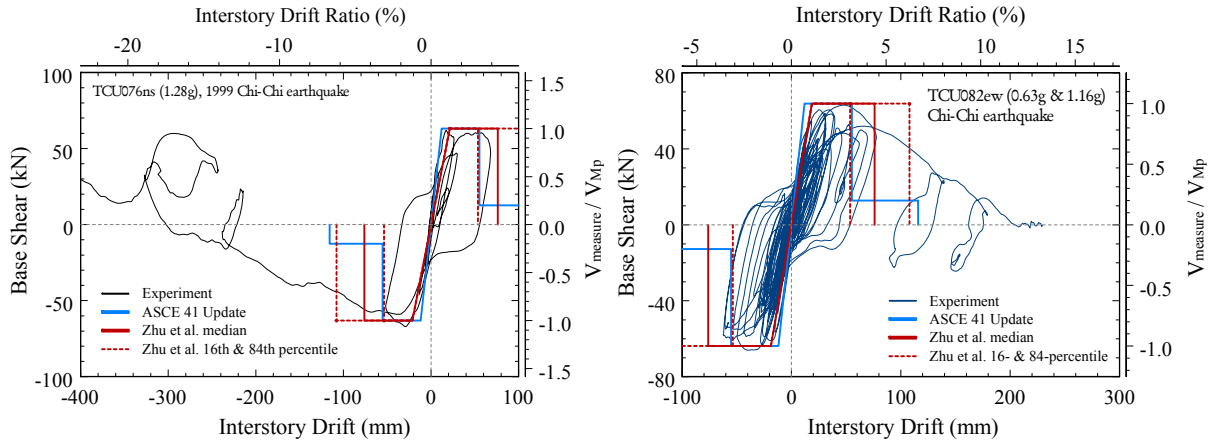
Figure 5.   Experimental hysteretic loops of flexure-shear critical columns in comparison with the ASCE/SEI 41-06 Update models and probabilistic force-deformation curves (Zhu et al., 2007) subjected to TCU076ns (left) and TCU082ew (right).
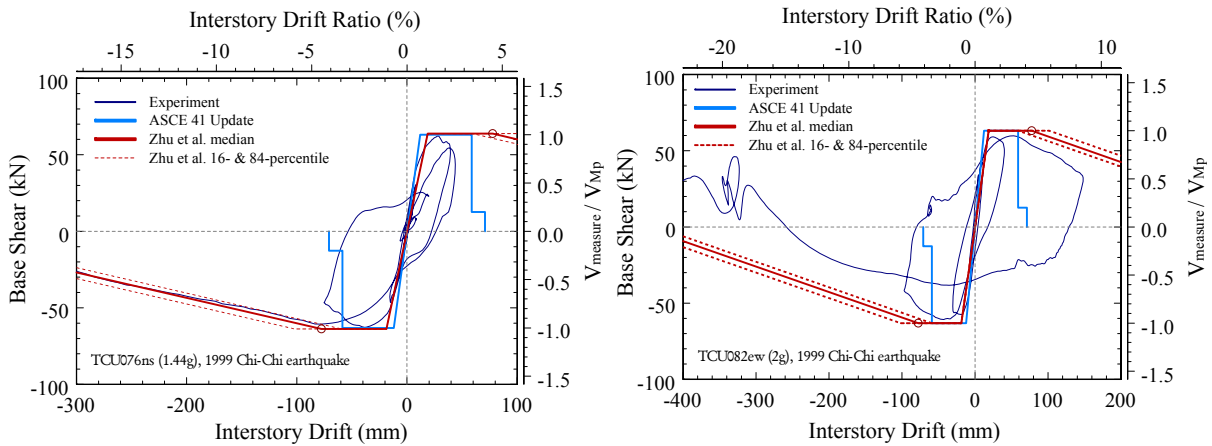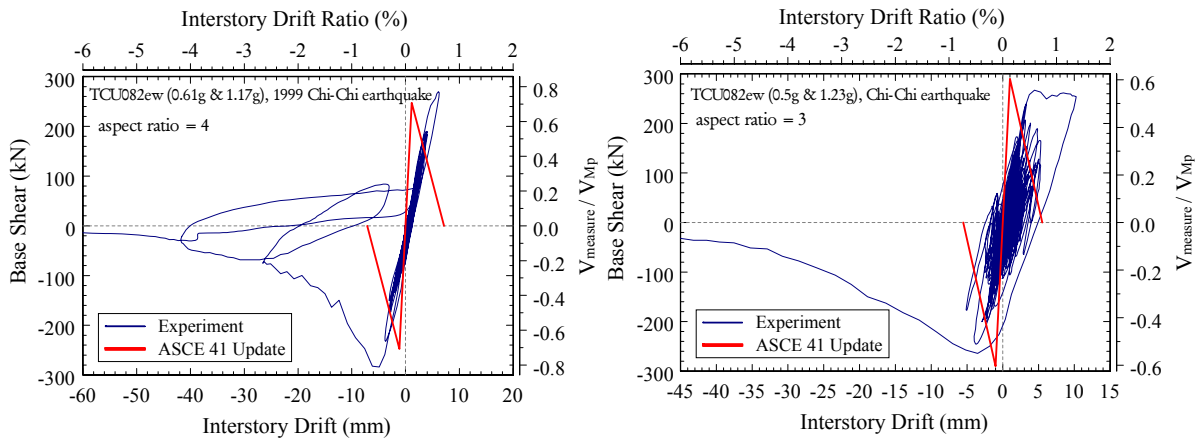

Figure 6.   Experimental hysteretic loops of flexure critical columns in comparison with the ASCE/SEI 41-06 Update models and probabilistic force-deformation curves (Zhu et al., 2007) subjected to TCU076ns (left) and TCU082ew (right).

Figure 7.   Experimental hysteretic loops of shear critical columns in comparison with the ASCE/SEI 41-06 Update models: aspect ratio = 4 (left) and 3 (right).

Conclusions

A representative set of shaking table tests resulting in dynamic axial collapse of reinforced concrete frames covering a good variety of column failure modes is reported. The test frames contained two identical columns subjected to near-fault and ordinary input motions. When subjected to a scaled version of the NS component of the TCU076 accelerogram (near-fault) or the EW component of the TCU082 accelerogram (ordinary) from the 1999 Chi-Chi earthquake, the columns with wide spacing of transverse reinforcement sustained shear and axial failure while the columns with closely spaced transverse reinforcement sustained flexural failure. Strengths and drift capacities of the test frames were compared with values calculated using published analytical models. The models contained in the ASCE/SEI 41-06 Update (2007) standard produced reasonably close estimates of strength but moderately conservative estimates of deformation capacity for the columns tested in this study. The probability-based model of Zhu et al. (2007) produced comparable predictive results with the ASCE/SEI 41-06 Update when mean minus one standard deviation deformation values were used in the analytical model. Subsequent studies of the authors will continue and focus on performance evaluation of the recently developed element models and dynamic simulation methods.

Acknowledgments

References

ASCE/SEI 41-06, 2007. *Seismic Rehabilitation of Existing Buildings*, America Society of Civil Engineers, Reston, V.A..

Elwood K.J., Matamoros A.B., Wallace J.W., Lehman D.E., Heintz J.A., Mitchell A..D., Moore M.A., Valley M.T., Lowes L.N., Comartin C.D., and Moehle J.P., 2007. Update to ASCE/SEI 41 Concrete Provisions, *Earthquake Spectra*, 23(3), 493-523.

Elwood K.J., and Moehle J.P., 2006. Idealized backbone model for existing reinforced concrete columns and comparisons with FEMA 356 criteria, *Structural Design of Tall and Special Buildings*, 15, 553-569.

Otani S., 1999. RC Building Damage Statistics and SDF Response with Design Seismic Forces, *Earthquake Spectra*, 15 (3), 485-501.

Yavari S., Elwood K.J., and Wu C.L., 2009. Collapse of a Nonductile Concrete Frame: Evaluation of Analytical Models, *Earthquake Engineering and Structural Dynamics*, 38 (2), 225-241.

Yang Y.S., Wu C.L., Loh C.H., Lin C.H., and Chao S.H., 2006. Dynamic Gravity Load Collapse of Non-ductile RC Frames II : Computational Approach, *the 100th Anniversary Earthquake Conference Commemorating the 1906 San Francisco Earthquake*, San Francisco, April 18-22.

Zhu L., Elwood K.J., and Haukaas T., 2007. Classification and Seismic Safety Evaluation of Existing Reinforced Concrete Columns, *Journal of Structural Engineering, ASCE*, 133 (9), 1316-1330.